This article has been accepted for publication in a future issue of this journal, but has not been fully edited. Content may change prior to final publication. Citation information: DOI 10.1109/TPWRD.2020.2974294, IEEE Transactions on Power Delivery

Time-domain Transmission Line Fault Location Method with Full Consideration of Distributed Parameters and Line Asymmetry

Dayou Lu, *Student Member*, *IEEE*, Yu Liu, *Member*, *IEEE*, Qifeng Liao, Binglin Wang, *Student Member*, *IEEE*, Wentao Huang, *Member*, *IEEE* and Xinze Xi

Abstract*— Accurate fault location reduces operating cost and outage time. This paper proposes a time-domain method to accurately locate faults in transmission lines, which only requires a very short data window (several milliseconds) during faults. First, the voltage distribution through the line during faults is accurately obtained by solving the matrix form partial differential equations using the proposed numerical scheme. The proposed numerical scheme is mathematically validated for the transmission line fault location problem, with the optimal selection of time and distance intervals to ensure stability and minimum solution error. Afterwards, the fault location is obtained via the extremum value of the voltage distribution. The method fully considers distributed parameters as well as asymmetry of the line. Extensive numerical experiments validated that (a) the proposed numerical scheme demonstrates advantages towards other numerical schemes; (b) the proposed method presents higher fault location accuracy compared to the existing method, independent of fault types, locations and impedances; and (c) the fault location accuracy is not sensitive towards fault inception angles, loading conditions, measurement errors and parameter errors. The proposed method works with relatively low sampling rates (80 samples per cycle) and is compatible with IEC 61850 standard in present digital substations.

***Index Terms*— time-domain fault location, distributed transmission line model, line asymmetry, short data window, IEC 61850**

I. Introduction

Accurate fault location minimizes the time spent searching for the fault and reduce the operating expense of the power system. Transmission line fault location techniques are extensively researched in existing literatures, mainly including frequency domain methods and time domain methods. Frequency domain methods usually use the fundamental frequency phasor measurements to calculate the fault location [1-4]. The main challenge of frequency domain methods is that the accuracy of the calculated phasors could be compromised especially during system transients. Consequently, a relatively long data window during the fault is usually required to ensure the accuracy of the fault location. For transmission lines with high-speed tripping techniques, the accessible data window is very short (sometimes several milli-seconds) [5]. To accurately locate faults with a short data window, researchers proposed time domain methods which can be further classified into time domain measurement based fault location methods and time domain model based fault location methods.

This work is sponsored by National Natural Science Foundation of China (No. 51807119, No. 11601329), Shanghai Pujiang Program (No. 18PJ1408100) and Key Laboratory of Control of Power Transmission and Conversion (SJTU), Ministry of Education (No. 2015AB04). Their support is greatly appreciated.

D. Lu, Y. Liu (corresponding author, liuyu.shanghaitech@gmail.com), Q. Liao and B. Wang are with the School of Information Science and Technology, ShanghaiTech University, Shanghai, China. D. Lu is also with the Shanghai Advanced Research Institute, Chinese Academy of Sciences; Shanghai Institute of Microsystem and Information Technology, Chinese Academy of Sciences; and University of Chinese Academy of Sciences. W. Huang is with the Department of Electrical Engineering, Shanghai Jiao Tong University (SJTU); and Key Laboratory of Control of Power Transmission and Conversion (SJTU), Ministry of Education. X. Xi is with the School of Electrical Engineering, Chongqing University; and Electric Power Research Institute of Yunnan Power Grid Co. Ltd.

For **time domain measurement based methods**, the most widely adopted methods are the traveling wave methods. Traveling wave methods find the distance between the line terminal and the fault location using the traveling wave velocity as well as the detected the arrival time of traveling waves [6-12]. The limitations of traveling wave methods are as follows. First, the wavefront detection reliability may not be guaranteed especially during faults with zero inception angles. In addition, the methods usually require a very high sampling rate to ensure the fault location accuracy.

For **time domain model based methods**, they analyze the relationship between fault location and the available measurements using the accurate model of transmission lines. These methods can be further classified according to whether the relationship is analytically expressed, including the methods of solving equations and the voltage methods.

Firstly, *the methods of solving equations* construct analytical equations describing the relationship between the fault location (the unknown variable) and the available measurements. With analytical expressions, the fault location problem becomes an equation-solving problem. To formulate the analytical equation in time domain, the lumped parameter transmission line model is usually utilized to approximate the fully distributed parameter model [13-15], which may result in compromised fault location accuracy. The utilization of the lumped parameter model is because the fully distributed parameter model in time domain is usually expressed in partial differential equations (PDEs), which are difficult to be rewritten into analytical equations with the fault location as an unknown variable.

Secondly, to avoid such formulation of analytical equations, researchers proposed *the voltage methods*. The methods first calculate the voltage distribution with measurements at either terminal respectively, and then the point of intersection of the two voltage distribution curves shows the fault location [16]. In order to solve the voltage distribution over the entire transmission line, one widely used model is the Bergeron model, which fully considers distributed inductance and capacitance [5, 17, 18]. The limitation of the traditional Bergeron model is the assumptions of lumped series resistance and zero shunt conductance. To consider the transmission line model with fully distributed parameters, the description using PDEs is introduced. The numerical solution of the PDEs achieves voltage methods fault location. For example, researchers proposed a fault location algorithm using the method of characteristics to solve the one-dimensional PDE [16]. However, the stability and minimum error conditions of existing numerical solutions are usually not mathematically verified. In this case, the method may not work well with user-defined time and distance intervals in a general transmission line system. In addition, existing time domain voltage methods usually utilize constant transformation matrices such as Clarke transformation and Karrenbauer's

transformation to decouple the three phase network. These transformations are based on the assumption of geometrically symmetrical structure of transmission lines. With asymmetrical transmission lines, the multi-phase models (the Bergeron model or models with PDEs) generally cannot be fully decoupled, which may affect the fault location accuracy.

This paper proposes a novel time domain transmission line fault location method which fully considers distributed parameters and asymmetry of transmission lines. The matrix form PDEs that describe the physical laws of the multi-phase transmission line are numerically solved to find the voltage distribution through the entire line. Afterwards, the fault location is obtained by finding the point of intersection of the voltage distribution curves. The effectiveness of the proposed numerical scheme is mathematically proved through the stability analysis and the error analysis. In addition, an optimal selection of distance and time intervals in solving the matrix form PDEs is derived to minimize the fault location error. Numerical experiments in a 300 km three phase AC transmission line system verify that the proposed fault location method presents higher fault location accuracy compared to existing approaches, with a short time window of 5 ms and a relatively low sampling rate of 80 samples per cycle (or 4 kHz for a power system with 50 Hz nominal frequency) according to IEC61850-9-2LE standard in digital substations.

The rest of the paper is organized as follows. Section II explains in detail the motivation of proposing a new numerical scheme. Section III mathematically derives the proposed numerical scheme and proves its effectiveness through stability analysis and error analysis. Section IV introduces the fault location methodology using the proposed numerical scheme. Section V and VI verifies the advantages of the proposed fault location method using numerical experiments. Section VII discusses the effects of different factors on the fault location accuracy. Section VIII draws a conclusion.

II. Background and Motivation of Proposing a New Numerical Scheme

This section introduces the background of the numerical solution of PDEs and the necessity of a new numerical scheme for fault location. Here a multi-conductor transmission line with the number of conductors *M* is selected as an example. The transmission line model in the matrix form PDEs fully considers distributed parameters and asymmetry of the transmission line, as follows,

$$\begin{aligned} \partial \boldsymbol{u}(x,t)/\partial x + \boldsymbol{L}\cdot\partial \boldsymbol{i}(x,t)/\partial t + \boldsymbol{R}\cdot\boldsymbol{i}(x,t) = \boldsymbol{0} \\ \partial \boldsymbol{i}(x,t)/\partial x + \boldsymbol{C}\cdot\partial \boldsymbol{u}(x,t)/\partial t + \boldsymbol{G}\cdot\boldsymbol{u}(x,t) = \boldsymbol{0} \end{aligned} \tag{1}$$

where $\boldsymbol{u}(x,t)=\left[u_1(x,t)\ \cdots\ u_M(x,t)\right]^{\mathrm{T}}$, $\boldsymbol{i}(x,t)=\left[i_1(x,t)\ \cdots\ i_M(x,t)\right]^{\mathrm{T}}$, $u_j(x,t)$ and $i_j(x,t)\ (j=1,2,...,M)$ are voltages and currents of phase j at distance x and time t (positive direction of the current is the same as the positive direction of x), $x\in[0,l]$ is the distance from the local terminal of the line, l is the length of the line, $\boldsymbol{0}$ is the M-dimensional zero vector, and $\boldsymbol{R}$, $\boldsymbol{L}$, $\boldsymbol{G}$ and $\boldsymbol{C}$ are the resistance, inductance, conductance and capacitance matrices per unit length. Note that the asymmetry of the transmission line can be fully considered since the structures of parameter matrices are without any assumptions.

To locate faults, the calculation of the voltage distributions is achieved by the numerical solution of the matrix form PDEs (1) using the finite difference method with various numerical schemes. In fact, the numerical solutions of PDEs with finite difference methods are well-known principles in mathematics. Specifically, the solutions of the transmission line PDEs have been studied in the field of transmission line modeling. *Djordjevic* [19] considered the transmission line as a finite section lumped parameter system and numerically solves the voltage and current in each section. The stability and error of the scheme were not mathematically proved but only summarized through numerical experiments. For the same scheme, *Paul* [20] considered the CFL condition (which claims that the domain of dependence of the PDE should be included in the domain of dependence of the numerical scheme [21]) as the necessary condition of stability. The error of the scheme is verified through the circuit theory with strong assumptions of lossless and geometrically symmetry transmission lines.

Besides the aforementioned limitations, there is an even more important reason why the existing numerical schemes (in the field of transmission line modeling or even mathematics) should be mathematically re-evaluated and reconsidered for the fault location problem, as follows. The transmission line modeling problem (*Problem 1*) is in purpose of solving the voltages and currents through the transmission line with complete information of the rest of the system as well as the initial states of the system. It usually takes the voltage and current distributions at the starting time as the initial condition and takes the certain functional relationship between voltages and currents at each terminal as the boundary condition (obtained from the rest of the system connected to the transmission line). The calculation is through the time direction. The problem is,

$$\begin{aligned} &\textit{Problem 1}: \textit{Given}\ \boldsymbol{u}(x,0),\boldsymbol{i}(x,0)\ \forall x\in[0,l]; \\ &\qquad f_1[\boldsymbol{u}(0,t),\boldsymbol{i}(0,t)]=0,\ f_2[\boldsymbol{u}(l,t),\boldsymbol{i}(l,t)]=0, \forall t\in[0,\ t_F] \\ &\qquad \textit{Find}\ \ \boldsymbol{u}(x,t),\boldsymbol{i}(x,t)\ \ \forall x\in[0,l], \forall t\in[0,\ t_F] \end{aligned}$$

On the other hand, the transmission line fault location problem (*Problem 2*) is in purpose of solving the voltages and currents through the transmission line with given voltages and currents measured at only one terminal of the line (typically without information of the rest of the system). It takes the local terminal instantaneous voltage and current measurements as the initial condition, and the voltage and current distributions at the starting time as the boundary condition. The calculation is through the distance direction. The problem is,

$$\begin{aligned} &\textit{Problem 2}: \textit{Given}\ \boldsymbol{u}(0,t),\boldsymbol{i}(0,t)\ \ \forall t\in[0,\ t_F]; \boldsymbol{u}(x,0),\boldsymbol{i}(x,0)\ \forall x\in[0,l] \\ &\qquad \textit{Find}\ \ \boldsymbol{u}(x,t),\boldsymbol{i}(x,t)\ \forall t\in[0,\ t_F], \forall x\in[0,l] \end{aligned}$$

Therefore, the aim of this paper is to propose an appropriate numerical scheme in order to solve *Problem 2* (existing numerical schemes usually solve *Problem 1*). Next, the proposed numerical scheme is derived in detail. The validity of the proposed numerical scheme is mathematically examined through stability analysis and error analysis.

III. Mathematical Derivation of the Proposed Numerical Scheme for Solving Voltage Distribution

In this section, the numerical solutions of (1) with appropriate numerical scheme are proposed. To numerically solve (1), the partial derivative terms of the PDE are rewritten

into terms in the difference form. With various difference forms, PDE can be numerically solved with various schemes [21]. Next, one needs to select a mesh for the interested area. For the transmission line system, the mesh consists of the distance grid (with the distance interval Δx) and the time grid (with the time interval Δt). Besides, one also needs to transform (1) into PDEs with a single vector variable, including the following two equivalent ways. The first way is to combine the two vector variables (the voltage and current vector variables) into one vector variable and convert (1) into a first order matrix form PDE,

$$\partial \boldsymbol{y}(x,t)/\partial x + \boldsymbol{A}_1 \cdot \partial \boldsymbol{y}(x,t)/\partial t + \boldsymbol{A}_2 \cdot \boldsymbol{y}(x,t) = \boldsymbol{0} \quad (2)$$

where $\boldsymbol{y} = [\boldsymbol{u} \;\; \boldsymbol{i}]^{\mathrm{T}}$, $\boldsymbol{A}_1 = [\boldsymbol{O} \;\; \boldsymbol{L};\; \boldsymbol{C} \;\; \boldsymbol{O}]$, $\boldsymbol{A}_2 = [\boldsymbol{O} \;\; \boldsymbol{R};\; \boldsymbol{G} \;\; \boldsymbol{O}]$ and $\boldsymbol{O}$ is the M-dimensional zero square matrix.

The second way is to eliminate one of the two vector variables and convert (1) into second order PDEs,

$$\partial^2 \boldsymbol{u}(x,t)/\partial x^2 = \boldsymbol{B}_1 \cdot \partial^2 \boldsymbol{u}(x,t)/\partial t^2 + \boldsymbol{B}_2 \cdot \partial \boldsymbol{u}(x,t)/\partial t + \boldsymbol{B}_3 \cdot \boldsymbol{u}(x,t) \quad (3a)$$

$$\partial^2 \boldsymbol{i}(x,t)/\partial x^2 = \boldsymbol{C}_1 \cdot \partial^2 \boldsymbol{i}(x,t)/\partial t^2 + \boldsymbol{C}_2 \cdot \partial \boldsymbol{i}(x,t)/\partial t + \boldsymbol{C}_3 \cdot \boldsymbol{i}(x,t) \quad (3b)$$

where $\boldsymbol{B}_1 = \boldsymbol{LC}$, $\boldsymbol{B}_2 = \boldsymbol{RC} + \boldsymbol{LG}$, $\boldsymbol{B}_3 = \boldsymbol{RG}$, $\boldsymbol{C}_1 = \boldsymbol{CL}$, $\boldsymbol{C}_2 = \boldsymbol{CR} + \boldsymbol{GL}$ and $\boldsymbol{C}_3 = \boldsymbol{GR}$.

Afterwards, three widely used explicit schemes are carefully studied to solve (2) or (3): the ordinary one-step explicit scheme to solve (2), the Lax-Wendroff scheme to solve (2), and the leap-frog scheme to solve (3). For each scheme, the explicit formulation of the solution is derived for calculating voltage distribution, followed by the stability analysis and the error analysis of each scheme. **Note that, the stability analysis and the error analysis are rigorous mathematical steps to theoretically ensure the effectiveness of the numerical scheme and to provide guidance on the optimal way of selecting the distance and time intervals for each scheme.**

A. Ordinary One-Step Explicit Scheme

The most straightforward and naive way to solve (2) is to use the explicit scheme with the first order difference form.

1) Derivation of Solution in Discretization Format

For (2), rewrite $\partial \boldsymbol{y}(x,t)/\partial x$ as the forward difference form to achieve the one step scheme. Rewrite $\partial \boldsymbol{y}(x,t)/\partial t$ as the central difference form. Equation (2) is rewritten as follows,

$$\left(\boldsymbol{Y}_{j+1}^{n} - \boldsymbol{Y}_{j}^{n}\right)/\Delta x + \boldsymbol{A}_1 \cdot \left(\boldsymbol{Y}_{j}^{n+1} - \boldsymbol{Y}_{j}^{n-1}\right)/2\Delta t + \boldsymbol{A}_2 \cdot \boldsymbol{Y}_{j}^{n} = \boldsymbol{0} \quad (4)$$

where the approximate numerical solution is expressed as the capital letter variable with the subscript j as the distance step number and the superscript n as the time step number (same definition through the paper). For example, the approximate numerical solution of variable $\boldsymbol{y}(x_j, t_j)$ is expressed as $\boldsymbol{Y}_j^n$, where $x_j = j\Delta x$, $t_j = n\Delta t$, $j = 1,2,...,N_x$ and $n = 1,2,...,N_t$.

The solution of $\boldsymbol{Y}_{j+1}^{n}$ is

$$\boldsymbol{Y}_{j+1}^{n} = \left(\boldsymbol{E} - \Delta x \boldsymbol{A}_2\right) \cdot \boldsymbol{Y}_{j}^{n} - \Delta x/2\Delta t \cdot \boldsymbol{A}_1 \cdot \left(\boldsymbol{Y}_{j}^{n+1} - \boldsymbol{Y}_{j}^{n-1}\right) \quad (5)$$

where $\boldsymbol{E}$ is the identity matrix with the dimension of $2M$.

Here the solution at (x_{j+1}, t_n) is expressed by three solutions at (x_j, t_{n-1}), (x_j, t_n) and (x_j, t_{n+1}). The entire voltage distribution can be solved step by step. The calculation direction is exactly corresponding to the requirement of problem 2.

2) Stability Analysis

The stable condition of a numerical scheme is derived with Fourier analysis [21]. Take the term of $(\lambda)^j e^{ik(n\Delta t)}$ as the Fourier series of the exact analytical solution at point (x_j, t_n), where k is the wave number of the Fourier series and i is the imaginary unit. Substitute the Fourier series into the numerical scheme, the amplification $|\lambda|$ is expressed with Δx, Δt and k. For k varying from negative infinity to positive infinity, the range of variables Δx and Δt that makes $|\lambda|$ always smaller than or equal to one is the stable condition.

For the ordinary one-step explicit scheme, consider the Fourier mode $\boldsymbol{y}_j^n = \left[(\lambda_1)^j e^{ik(n\Delta t)}, \cdots, (\lambda_{2M})^j e^{ik(n\Delta t)}\right]^{\mathrm{T}} = (\boldsymbol{\lambda})^j \odot \boldsymbol{e}^{ik(n\Delta t)}$, where $\odot$ expresses element-wise product, $(\boldsymbol{\lambda})^j = \left[(\lambda_1)^j \;\; \cdots \;\; (\lambda_{2M})^j\right]^{\mathrm{T}}$, $\boldsymbol{e}^{ik(n\Delta t)} = e^{ik(n\Delta t)} \cdot \boldsymbol{1}$ and $\boldsymbol{1}$ is $2M$-dimensional unit vector. Substitute them into (4),

$$(\boldsymbol{\lambda} - \boldsymbol{1})/\Delta x + \boldsymbol{A}_1 \cdot \left[\boldsymbol{e}^{ik(\Delta t)} - \boldsymbol{e}^{-ik(\Delta t)}\right]/2\Delta t + \boldsymbol{A}_2 \cdot \boldsymbol{1} = 0 \quad (6)$$

Note that $e^{ik(\Delta t)} - e^{-ik(\Delta t)} = i \cdot 2\sin(k\Delta t)$, the solution of $\boldsymbol{\lambda}$ is,

$$\boldsymbol{\lambda} = \boldsymbol{1} - \Delta x/\Delta t \cdot \left[i \cdot \sin(k\Delta t)\right] \boldsymbol{A}_1 \cdot \boldsymbol{1} - \Delta x \boldsymbol{A}_2 \cdot \boldsymbol{1} \quad (7)$$

The maximum amplification $|\lambda_p|$ $(p = 1 \sim 2M)$ for all k is $|\lambda_p| = \sqrt{\left(\frac{\Delta x}{\Delta t}\sum_{q=1}^{2M} A_{1pq}\right)^2 + \left(1 - \Delta x \sum_{q=1}^{2M} A_{2pq}\right)^2}$, where A_{1pq} and A_{2pq} represent matrix elements at row p and column q of $\boldsymbol{A}_1$ and $\boldsymbol{A}_2$.

Therefore, the stable condition is,

$$\Delta x \le \min\left\{2\Delta t^2 \sum_{q=1}^{2M} A_{2pq} \Big/ \left[\left(\sum_{q=1}^{2M} A_{1pq}\right)^2 + \left(\Delta t \sum_{q=1}^{2M} A_{2pq}\right)^2\right],\ p = 1 \sim 2M\right\} \quad (8)$$

With typical line parameters of $\boldsymbol{A}_1$ and $\boldsymbol{A}_2$, since the typical sampling interval Δt of instantaneous measurements is in the order of 10^{-4} seconds or less, the stable condition requires that Δx is approximately in the order of $10^0 \sim 10^1$ meters or less. In fact, since the length of a typical transmission line is in the order of $10^4 \sim 10^5$ meters, the aforementioned Δx will result in overwhelmed number of meshes. In addition, to calculate voltage distribution through the entire line, N_t should be larger than N_x (details of this phenomenon will be introduced in section IV). In this case, this mesh requires an extremely long data window (in the order of seconds) and is not applicable in practice. Therefore, this scheme is considered as an unstable scheme for transmission line fault location problem. The most straightforward ordinary one-step explicit scheme is not quite applicable for fault location.

3) Error Analysis

Since this scheme is considered unstable, the error analysis of this scheme will not be provided.

B. Improved One-Step Scheme: Lax-Wendroff Scheme

Another one-step scheme with improved stability is the Lax-Wendreoff scheme. The main idea of the Lax-Wendroff scheme is to keep the second order terms of Taylor expansion in the process of approximating the partial derivatives.

This article has been accepted for publication in a future issue of this journal, but has not been fully edited. Content may change prior to final publication. Citation information: DOI 10.1109/TPWRD.2020.2974294, IEEE Transactions on Power Delivery

1) Derivation of Solution in Discretization Format

Take the second order Taylor expansion of $\boldsymbol{y}(x_{j+1},t_n)$ with respect to the distance *x*,

$$\boldsymbol{y}(x_{j+1},t_n)=\boldsymbol{y}(x,t)+\Delta x\boldsymbol{y}_x(x,t)+\Delta x^2/2\cdot\boldsymbol{y}_{xx}(x,t)=\boldsymbol{y}(x,t)+\Delta x\left[-\boldsymbol{A}_1\boldsymbol{y}_t(x,t)-\boldsymbol{A}_2\boldsymbol{y}(x,t)\right]+\Delta x^2/2\cdot\left[\boldsymbol{A}_1\boldsymbol{A}_1\boldsymbol{y}_{tt}(x,t)+(\boldsymbol{A}_1\boldsymbol{A}_2+\boldsymbol{A}_2\boldsymbol{A}_1)\boldsymbol{y}_t(x,t)+\boldsymbol{A}_2\boldsymbol{A}_2\boldsymbol{y}(x,t)\right] \quad (9)$$

where the subscripts of $\boldsymbol{y}$ indicate partial derivatives of $\boldsymbol{y}$ with respect to the subscript variables.

Use central difference form to approximate time partial derivatives and rewrite (9),

$$\boldsymbol{Y}_{j+1}^n=\boldsymbol{Y}_j^n+\Delta x\left[-\boldsymbol{A}_1\left(\boldsymbol{Y}_j^{n+1}-\boldsymbol{Y}_j^{n-1}\right)/2\Delta t-\boldsymbol{A}_2\boldsymbol{Y}_j^n\right]+\Delta x^2/2\cdot\left[\boldsymbol{A}_1\boldsymbol{A}_1\left(\boldsymbol{Y}_j^{n+1}-2\boldsymbol{Y}_j^n+\boldsymbol{Y}_j^{n-1}\right)/\Delta t^2+\left(\boldsymbol{A}_1\boldsymbol{A}_2+\boldsymbol{A}_2\boldsymbol{A}_1\right)\left(\boldsymbol{Y}_j^{n+1}-\boldsymbol{Y}_j^{n-1}\right)/2\Delta t+\boldsymbol{A}_2\boldsymbol{A}_2\boldsymbol{Y}_j^n\right] \quad (10)$$

Therefore, the numerical solution of $\boldsymbol{Y}_{j+1}^n$ is,

$$\begin{aligned}\boldsymbol{Y}_{j+1}^n=&\left(\boldsymbol{E}-\Delta x\boldsymbol{A}_2-\Delta x^2/\Delta t^2\cdot\boldsymbol{A}_1\boldsymbol{A}_1+\Delta x^2/2\cdot\boldsymbol{A}_2\boldsymbol{A}_2\right)\boldsymbol{Y}_j^n\\&+\left[-\Delta x/2\Delta t\cdot\boldsymbol{A}_1+\Delta x^2/2\Delta t^2\cdot\boldsymbol{A}_1\boldsymbol{A}_1+\Delta x^2/4\Delta t\cdot\left(\boldsymbol{A}_1\boldsymbol{A}_2+\boldsymbol{A}_2\boldsymbol{A}_1\right)\right]\boldsymbol{Y}_j^{n+1}\\&+\left[\Delta x/2\Delta t\cdot\boldsymbol{A}_1+\Delta x^2/2\Delta t^2\cdot\boldsymbol{A}_1\boldsymbol{A}_1-\Delta x^2/4\Delta t\cdot\left(\boldsymbol{A}_1\boldsymbol{A}_2+\boldsymbol{A}_2\boldsymbol{A}_1\right)\right]\boldsymbol{Y}_j^{n-1}\end{aligned} \quad (11)$$

2) Stability Analysis

Similarly, consider the Fourier mode $\boldsymbol{y}_j^n=(\boldsymbol{\lambda})^j\odot\boldsymbol{e}^{ik(n\Delta t)}$, substitute it into (11),

$$\begin{aligned}\boldsymbol{\lambda}=&\left(\boldsymbol{E}-\Delta x\boldsymbol{A}_2-\Delta x^2/\Delta t^2\cdot\boldsymbol{A}_1\boldsymbol{A}_1+\Delta x^2/2\cdot\boldsymbol{A}_2\boldsymbol{A}_2\right)\boldsymbol{1}+\cos(k\Delta t)\left[\Delta x^2/\Delta t^2\cdot\boldsymbol{A}_1\boldsymbol{A}_1\right]\boldsymbol{1}\\&+i\sin(k\Delta t)\left[-\Delta x/\Delta t\cdot\boldsymbol{A}_1+\Delta x^2/2\Delta t\cdot\left(\boldsymbol{A}_1\boldsymbol{A}_2+\boldsymbol{A}_2\boldsymbol{A}_1\right)\right]\boldsymbol{1}\end{aligned} \quad (12)$$

Consider the maximum amplification $|\lambda_p|\,(p=1\sim 2M)$. With fixed Δx and Δt, λ_p is an ellipse in the complex plane with variable *k*. The maximum $|\lambda_p|$ is obtained when $\cos(k\Delta t)=\pm1$, $\sin(k\Delta t)=0$, the value is $\max\left\{\left|1-\Delta x\sum_{q=1}^{2M}(\boldsymbol{A}_2)_{pq}+\frac{\Delta x^2}{2}\cdot\sum_{q=1}^{2M}(\boldsymbol{A}_2\boldsymbol{A}_2)_{pq}\right|,\left|1-\Delta x\sum_{q=1}^{2M}(\boldsymbol{A}_2)_{pq}+\frac{\Delta x^2}{2}\cdot\sum_{q=1}^{2M}(\boldsymbol{A}_2\boldsymbol{A}_2)_{pq}-2\frac{\Delta x^2}{\Delta t^2}\cdot\sum_{q=1}^{2M}(\boldsymbol{A}_1\boldsymbol{A}_1)_{pq}\right|\right\}$.

Therefore, the stable condition is

$$\Delta x\le\min\left\{\left[-\sum_{q=1}^{2M}(\boldsymbol{A}_2)_{pq}+\sqrt{\left(\sum_{q=1}^{2M}(\boldsymbol{A}_2)_{pq}\right)^2+8\left(\frac{2}{\Delta t^2}\sum_{q=1}^{2M}(\boldsymbol{A}_1\boldsymbol{A}_1)_{pq}-\frac{1}{2}\sum_{q=1}^{2M}(\boldsymbol{A}_2\boldsymbol{A}_2)_{pq}\right)}\right]\Big/\left(2\left(\frac{2}{\Delta t^2}\sum_{q=1}^{2M}(\boldsymbol{A}_1\boldsymbol{A}_1)_{pq}-\frac{1}{2}\sum_{q=1}^{2M}(\boldsymbol{A}_2\boldsymbol{A}_2)_{pq}\right),2\sum_{q=1}^{2M}(\boldsymbol{A}_2)_{pq}\Big/\sum_{q=1}^{2M}(\boldsymbol{A}_2\boldsymbol{A}_2)_{pq},p=1\sim2M\right\} \quad (13)$$

With typical parameters, equation (13) requires that the ratio of the distance interval and time interval in the order of 10^8 meters per second. The corresponding minimum requirement of the available data window is acceptable (in the order of milli-second). Therefore, proper selection of Δx and Δt could ensure stability of this scheme.

3) Error Analysis

The error of a numerical scheme is estimated by substituting the exactly analytical solution into the difference equation [21]. The truncation error can be calculated as the difference between the left side and the right side of (10) divided by Δx, after substituting the Taylor expansions of the exactly analytical solution into the equation for each term. The truncation error is,

$$\begin{aligned}\boldsymbol{T}_j^n=&\left(\boldsymbol{y}_{j+1}^n-\boldsymbol{y}_j^n\right)/\Delta x+\boldsymbol{A}_1\left(\boldsymbol{y}_j^{n+1}-\boldsymbol{y}_j^{n-1}\right)/2\Delta t+\boldsymbol{A}_2\boldsymbol{y}_j^n-\Delta x/2\cdot\left[\boldsymbol{A}_1\boldsymbol{A}_1\left(\boldsymbol{y}_j^{n+1}-2\boldsymbol{y}_j^n+\boldsymbol{y}_j^{n-1}\right)/\Delta t^2+\left(\boldsymbol{A}_1\boldsymbol{A}_2+\boldsymbol{A}_2\boldsymbol{A}_1\right)\left(\boldsymbol{y}_j^{n+1}-\boldsymbol{y}_j^{n-1}\right)/2\Delta t+\boldsymbol{A}_2\boldsymbol{A}_2\boldsymbol{y}_j^n\right]=\left\{-\Delta x\Delta t^2/24\cdot\boldsymbol{A}_1\boldsymbol{A}_1\cdot\boldsymbol{y}_{ttt}+\left[\Delta t^2/6\cdot\boldsymbol{A}_1-\Delta x\Delta t^2/12\cdot\left(\boldsymbol{A}_1\boldsymbol{A}_2+\boldsymbol{A}_2\boldsymbol{A}_1\right)\right]\boldsymbol{y}_{ttt}\right\}_j^n+O(\Delta x^2)+O(\Delta t^4)\end{aligned} \quad (14)$$

To minimize the truncation error, it requires that the coefficients before $\boldsymbol{y}_{tttt}$ and $\boldsymbol{y}_{ttt}$ are close to zero. Obviously, there is no such selection of non-zero Δx and Δt that could make either coefficient zero. In this case, the high accuracy usually comes with extremely short distance and time interval, which may increase the computational burden of the algorithm.

C. Two-Step Scheme: Leap-frog Scheme

To further consider the minimized truncation error, the two-step leap-frog scheme is introduced to solve (3). Leap-frog scheme rewrites both time and distance derivatives with the second order central difference form. Here the solution of (3a) is taken as an example and the solution of (3b) is similar.

1) Derivation of Solution in Discretization Format

Rewrite (3a) with the central difference form,

$$\begin{aligned}\left(\boldsymbol{U}_{j+1}^n-2\boldsymbol{U}_j^n+\boldsymbol{U}_{j-1}^n\right)/\Delta x^2=&\boldsymbol{B}_1\left(\boldsymbol{U}_j^{n+1}-2\boldsymbol{U}_j^n+\boldsymbol{U}_j^{n-1}\right)/\Delta t^2\\&+\boldsymbol{B}_2\left(\boldsymbol{U}_j^{n+1}-\boldsymbol{U}_j^{n-1}\right)/2\Delta t+\boldsymbol{B}_3\boldsymbol{U}_j^n\end{aligned} \quad (15)$$

The numerical solution of $\boldsymbol{U}_{j+1}^n$ is

$$\begin{aligned}\boldsymbol{U}_{j+1}^n=&-\boldsymbol{U}_{j-1}^n+\left(2\boldsymbol{E}-2\Delta x^2/\Delta t^2\cdot\boldsymbol{B}_1+\Delta x^2\boldsymbol{B}_3\right)\boldsymbol{U}_j^n+\left(\Delta x^2/\Delta t^2\cdot\boldsymbol{B}_1\right.\\&\left.-\Delta x^2/2\Delta t\cdot\boldsymbol{B}_2\right)\boldsymbol{U}_j^{n-1}+\left(\Delta x^2/\Delta t^2\cdot\boldsymbol{B}_1+\Delta x^2/2\Delta t\cdot\boldsymbol{B}_2\right)\boldsymbol{U}_j^{n+1}\end{aligned} \quad (16)$$

2) Stability Analysis

Consider $\boldsymbol{u}_j^n=\left[(\lambda_1)^j e^{ik(n\Delta t)}\ \cdots\ (\lambda_M)^j e^{ik(n\Delta t)}\right]^{\mathrm{T}}=(\boldsymbol{\lambda})^j\odot\boldsymbol{e}^{ik(n\Delta t)}$. Substitute it into (15),

$$\begin{aligned}\boldsymbol{\lambda}-2\cdot\boldsymbol{1}+\boldsymbol{\lambda}^{-1}=&2\left(\cos(k\Delta t)-1\right)\Delta x^2/\Delta t^2\cdot\boldsymbol{B}_1\cdot\boldsymbol{1}\\&+\Delta x^2\cdot\boldsymbol{B}_3\cdot\boldsymbol{1}+i\cdot\sin(k\Delta t)\Delta x^2/\Delta t\cdot\boldsymbol{B}_2\cdot\boldsymbol{1}\end{aligned} \quad (17)$$

The solution of amplification $|\lambda_p|$ is,

$$|\lambda_p|=\left|b_p\pm\sqrt{b_p{}^2-4}\right|/2 \quad (18)$$

where $b_p=2+\frac{\Delta x^2}{\Delta t^2}\cdot\left[2\sum_{q=1}^{M}B_{1pq}\left(\cos(k\Delta t)-1\right)+\Delta t\sum_{q=1}^{M}B_{2pq}\left(i\cdot\sin(k\Delta t)\right)\right]+\Delta x^2\sum_{q=1}^{M}B_{3pq}$.

Typical selection of Δt could be in the order of 10^{-4} seconds or less. In this case, b_p can be approximated as a real number $2+2\Delta x^2/\Delta t^2\cdot\sum_{q=1}^{M}B_{1pq}\cdot\left(\cos(k\Delta t)-1\right)$. One can observe from (18) that $|\lambda_p|=1$ if $|b_p|\le2$ and $|\lambda_p|>1$ if $|b_p|>2$. Therefore, the stable condition is $2\Delta x^2/\Delta t^2\cdot\sum_{q=1}^{M}B_{1pq}\le2$, or

$$\Delta x^2/\Delta t^2\le\min\left\{1\Big/\sum_{q=1}^{M}B_{1pq},p=1\sim M\right\} \quad (19)$$

Strictly speaking, even equation (19) is satisfied, b_p could still be slightly larger than 1 in extreme cases. One example is $b_p=2+\Delta x^2\sum_{q=1}^{M}B_{3pq}$ when $k\Delta t=0,\pm2\pi,\cdots$. However, the maximum amplification $|\lambda_p|$ in the extreme cases is only a little larger than one (less than 1.002 with intervals satisfying (19) and typical line parameters). In practice, such amplification will not cause stability issues and the solution will maintain correctness within finite calculation steps [21]. Therefore, for transmission line fault location, it is also considered as a stable scheme.

This article has been accepted for publication in a future issue of this journal, but has not been fully edited. Content may change prior to final publication. Citation information: DOI 10.1109/TPWRD.2020.2974294, IEEE Transactions on Power Delivery

3) Error Analysis

Similarly, consider the truncation error with (15),

$$\begin{aligned}&\boldsymbol{T}_j^n=\left(\boldsymbol{U}_{j+1}^n-2\boldsymbol{U}_j^n+\boldsymbol{U}_{j-1}^n\right)\Big/\Delta x^2-\boldsymbol{B}_1\left(\boldsymbol{U}_j^{n+1}-2\boldsymbol{U}_j^n+\boldsymbol{U}_j^{n-1}\right)\Big/\Delta t^2-\boldsymbol{B}_2\left(\boldsymbol{U}_j^{n+1}\right.\\&\left.-\boldsymbol{U}_j^{n-1}\right)\Big/2\Delta t-\boldsymbol{B}_3\boldsymbol{u}_j^n=\left[\boldsymbol{u}_{xx}-\boldsymbol{B}_1\boldsymbol{u}_{tt}-\boldsymbol{B}_3\boldsymbol{u}+\Delta x^2/12\cdot\boldsymbol{u}_{xxxx}-\Delta t^2/12\cdot\boldsymbol{B}_1\boldsymbol{u}_{tttt}-\boldsymbol{B}_2\right.\\&\left.\cdot\left(\boldsymbol{u}_t+\Delta t^2/6\cdot\boldsymbol{u}_{ttt}\right)\right]_j^n+O\left(\Delta x^4\right)+O\left(\Delta t^4\right)=\left\{\left(\Delta x^2/12\cdot\boldsymbol{B}_1\boldsymbol{B}_1-\Delta t^2/12\cdot\boldsymbol{B}_1\right)\cdot\boldsymbol{u}_{tttt}\right.\\&\left.+\left[\Delta x^2/12\cdot\left(\boldsymbol{B}_1\boldsymbol{B}_2+\boldsymbol{B}_2\boldsymbol{B}_1\right)-\Delta t^2/6\cdot\boldsymbol{B}_2\right]\cdot\boldsymbol{u}_{ttt}+\Delta x^2/12\cdot\left(\boldsymbol{B}_1\boldsymbol{B}_3+\boldsymbol{B}_2\boldsymbol{B}_2+\boldsymbol{B}_3\boldsymbol{B}_1\right)\right.\\&\left.\cdot\boldsymbol{u}_{tt}+\Delta x^2\Big/12\cdot\left(\boldsymbol{B}_2\boldsymbol{B}_3+\boldsymbol{B}_3\boldsymbol{B}_2\right)\cdot\boldsymbol{u}_t+\Delta x^2/12\cdot\boldsymbol{B}_3\boldsymbol{B}_3\cdot\boldsymbol{u}\right\}_j^n+O\left(\Delta x^4\right)+O\left(\Delta t^4\right)\end{aligned}\tag{20}$$

To minimize the truncation error, it requires that the coefficients before $\boldsymbol{u}_{tttt}$, $\boldsymbol{u}_{ttt}$, $\boldsymbol{u}_{tt}$, $\boldsymbol{u}_t$ and $\boldsymbol{u}$ are close to zero. The minimum of the coefficient before $\boldsymbol{u}_{tttt}$ could be achieved if one selects Δx and Δt that satisfy the equality constraints in (19). Such selection of intervals also minimizes the coefficient before $\boldsymbol{u}_{ttt}$. Therefore, this scheme achieves a minimum truncation with reasonable selection of intervals.

In conclusion, the leap-frog scheme is a stable scheme which provides strict guidance for selection of the intervals. Consider both the stable condition and the minimum error condition, the best selection of Δx and Δt should satisfy,

$$\Delta x/\Delta t=Const\tag{21}$$

where $Const=\min\left\{1\Big/\sqrt{\sum_{q=1}^{M}B_{1pq}},p=1\sim M\right\}$.

Here the error of the solution is also verified by substitute the exactly analytical solution as $\boldsymbol{u}(j,n)=\boldsymbol{U}_j^n-\boldsymbol{e}_j^n$ into (15),

$$\begin{aligned}&\left|\boldsymbol{e}_{j+1}^n+\boldsymbol{e}_{j-1}^n\right|=\left|\left(2\boldsymbol{E}-2\Delta x^2/\Delta t^2\cdot\boldsymbol{B}_1+\Delta x^2\boldsymbol{B}_3\right)\boldsymbol{e}_j^n+\left(\Delta x^2/\Delta t^2\cdot\boldsymbol{B}_1+\right.\right.\\&\left.\left.\Delta x^2/2\Delta t\cdot\boldsymbol{B}_2\right)\boldsymbol{e}_j^{n+1}+\left(\Delta x^2/\Delta t^2\cdot\boldsymbol{B}_1-\Delta x^2/2\Delta t\cdot\boldsymbol{B}_2\right)\boldsymbol{e}_j^{n-1}-\Delta x^2\boldsymbol{T}_j^n\right|\le\left(2\boldsymbol{E}\right.\\&\left.-2\Delta x^2/\Delta t^2\cdot\boldsymbol{B}_1+\Delta x^2\boldsymbol{B}_3\right)\boldsymbol{E}_j+\left(\Delta x^2/\Delta t^2\cdot\boldsymbol{B}_1+\Delta x^2/2\Delta t\cdot\boldsymbol{B}_2\right)\boldsymbol{E}_j+\left(\boldsymbol{B}_1\right.\\&\left.\cdot\Delta x^2/\Delta t^2-\Delta x^2/2\Delta t\cdot\boldsymbol{B}_2\right)\boldsymbol{E}_j+\Delta x^2\left|\boldsymbol{T}_j^n\right|=2\boldsymbol{E}_j+\Delta x^2\left|\boldsymbol{T}_j^n\right|+\Delta x^2\boldsymbol{B}_3\boldsymbol{E}_j\end{aligned}\tag{22}$$

where $\boldsymbol{e}_j^n$ is the error of $\boldsymbol{U}_j^n$, $\boldsymbol{E}_j=\max\left\{\left|\boldsymbol{e}_j^n\right|,n=1,2,3,\cdots\right\}$.

Consider that $\boldsymbol{E}_1=\boldsymbol{E}_2=0$ and $\boldsymbol{E}_{j+1}\ge\boldsymbol{E}_j$ [21], the max error of the solution in distance step j+1 is,

$$\boldsymbol{E}_{j+1}\le\left[2\Big/\left(j\Delta x\right)^2\cdot\boldsymbol{E}-\boldsymbol{B}_3\right]^{-1}\bar{\boldsymbol{T}}\tag{23}$$

where $\bar{\boldsymbol{T}}=\max\left\{\left|\boldsymbol{T}_j^n\right|,\ j=1,2,3,\cdots;n=1,2,3,\cdots\right\}$.

For the last step, $j\Delta x$ is the length of the transmission line, then the error of the solution is in direct proportion to the truncation error. Therefore, the error of the scheme converges to zero when the interval approaches zero.

Note that, the leap-frog scheme is a two-step scheme and requires an additional starting condition (at distance Δx) which can be obtained by any one-step scheme. Here, the Lax-Wendroff scheme (which is also a stable scheme) is selected to calculate the additional starting condition.

In conclusion, for three schemes derived in this section, the ordinary one step explicit scheme (the simplest scheme for a PDE) is not stable for transmission line fault location problem. The Lax-Wendroff scheme is a stable scheme, but cannot mathematically achieve the minimum truncation error. **The best solution, the leap-frog scheme, is a stable scheme also achieves minimum truncation error with an optimal selection of intervals.**

IV. Methodology of the Fault Location by Applying the Proposed Numerical Scheme

Here the voltage method is applied to find the location of the fault. The validity of the voltage methods comes from the fact that the voltage at fault location is the extremum value of the voltage distribution through the entire transmission line. The voltage distribution through the transmission line can be solved using the proposed numerical scheme with the initial condition and boundary condition. Here the initial condition $\boldsymbol{u}(0,t)$ and $\boldsymbol{i}(0,t)$ can be directly obtained. The boundary condition $\boldsymbol{u}(x,0)$ and $\boldsymbol{i}(x,0)$ is approximated by,

$$\begin{aligned}\boldsymbol{u}(x,0)&=\left(l-x\right)/l\cdot\boldsymbol{u}(0,0)+x/l\cdot\boldsymbol{u}(l,0)\\\boldsymbol{i}(x,0)&=\left(l-x\right)/l\cdot\boldsymbol{i}(0,0)+x/l\cdot\boldsymbol{i}(l,0)\end{aligned}\tag{24}$$

After calculating the voltage distribution through the line from either terminal independently, the next step is to find the fault location from the intersection of the two calculated voltage distributions. To ensure the robustness of the algorithm, instead of using the voltage distribution curves at one instant of time, the summation of the voltage distribution curves at different time steps is considered and the point of intersection of the two summed voltage distribution curves is the fault location [5]. The fault location x can be obtained by solving the following minimization problem,

$$\min_x\sum_{t=0}^{t_d}f\left(x,t\right)\tag{25}$$

where $f\left(x,t\right)=\left|u^{(k)}\left(x,t\right)-u^{(m)}\left(x,t\right)\right|$, $u^{(k)}\left(x,t\right)$ and $u^{(m)}\left(x,t\right)$ are voltage distributions calculated with measurements at terminals k and m respectively, t_d is the summation window. For M phase transmission line system, voltage distribution for fault location can be selected as $u\left(x,t\right)=u_1\left(x,t\right)-\sum_{p=2}^{M}u_p\left(x,t\right)\Big/\left(M-1\right)$ to consider all types of faults [22].

Next, the computational complexity of the proposed scheme is discussed. In fact, the numerical scheme in (16) consists of only a limited number of matrix-vector multiplications and summations, and no matrix inverse is required. The computation complexity of the proposed method mainly comes from the high distance resolution of the voltage distribution (a small distance interval leads to a large number of calculation steps). To reduce the computation complexity, a two-iteration fault location algorithm is designed as shown in Figure 1 (a) [16]. For the first iteration, the approximate fault location $l_{f,iteration1}$ is calculated inside the overall transmission line $[0,l]$ using a relatively large distance interval $\Delta x_{iteration1}$. For the second iteration, the accurate fault location $l_{f,iteration2}$ is further refined inside the small transmission line segment $[l_{f,iteration1}-\Delta x_{iteration1},\ l_{f,iteration1}+\Delta x_{iteration1}]$ using a relatively small distance interval $\Delta x_{iteration2}$. For the first iteration, the distribution of currents through the line also needs to be solved, to provide the initial condition for the second fault location iteration. With the same fault location resolution ($\Delta x_{iteration2}$), compared to the original one-iteration algorithm, the two-iteration algorithm reduces the number of calculation steps

This article has been accepted for publication in a future issue of this journal, but has not been fully edited. Content may change prior to final publication. Citation information: DOI 10.1109/TPWRD.2020.2974294, IEEE Transactions on Power Delivery

from $l/\Delta x_{iteration2}$ to $(l/\Delta x_{iteration1}+2\Delta x_{iteration1}/\Delta x_{iteration2})$. The flow chart of the fault location algorithm is shown in Figure 2.

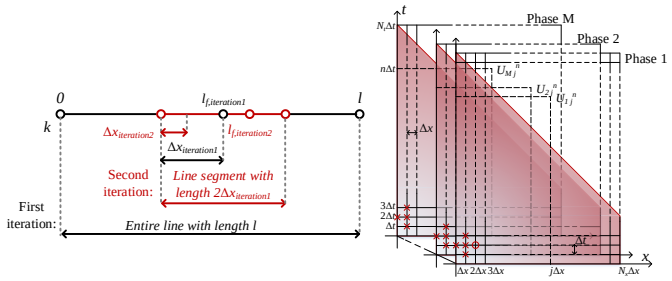

(a) Two iterations of the algorithm (b) The mesh for leap-frog scheme

Figure. 1. Details of the fault location algorithm

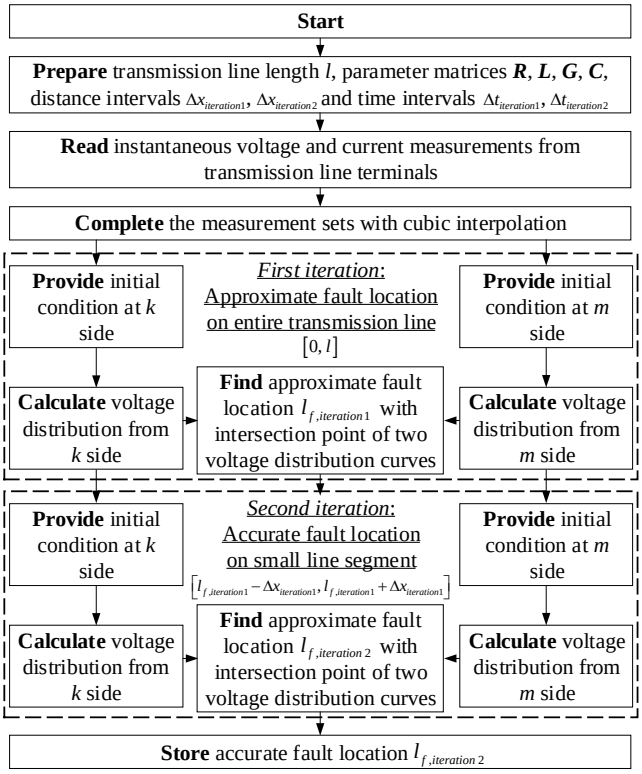

Figure 2. Flow chart of the proposed fault location algorithm

In addition, the data window for determining the fault location should be longer than a certain value which is proportional to the total length of the line. For example, the mesh to solve the voltage distribution of an M phase transmission line in iteration 1 is shown in Figure 1 (b). The horizontal axis x represents distance, the vertical axis t represents time and the third axis shows meshes for M phases. Take the node marked with circle in phase 1 as an example. The voltage of this node is calculated with $4M$ nodes marked with crosses in all M phases. Therefore, the voltages that could be solved are marked as the shaded red area. If $N_t < N_x$, the voltage distribution in the distance interval of $\left[(N_t+1)\Delta x, N_x\Delta x\right]$ cannot be solved. Therefore, the requiring data window should satisfy $N_t \geq N_x$. In this case, the summation window t_d is $(N_t - N_x)\Delta t$. Note that, the selection of Δx and Δt should satisfy (21) to ensure stable condition and minimum truncation error. Therefore, the minimum time window is $line\ length/Const$. In practice, since the value of *Const* is close to the speed of light, this minimum time window can usually be satisfied.

V. Numerical Validation of the Proposed Method: Comparison of Three Numerical Schemes

In this section, the aforementioned three numerical schemes are validated using numerical experiments, to prove the effectiveness of the proposed leap-frog scheme. The example test system shown in Figure 3 (a) is built in PSCAD/EMTDC. The line of interest is a 300 km, 500 kV three phase transmission line, with the system nominal frequency of 50 Hz. Here the frequency dependent transmission line model in PSCAD/EMTDC is utilized to ensure the validity of the simulated voltage and current waveforms during different fault events. The tower structure of the entire transmission line and the arrangement of phase conductors are shown in Figure 3 (b). One can observe that the transmission line is geometrically asymmetrical (for example, the mutual parameters among phases are not exactly the same). The phase angle difference between the two equivalent sources is 20°. Three phase voltage and current instantaneous measurements are installed at both terminals of the transmission line, with 80 samples per cycle (4 kilo-samples per second) sampling rate according to IEC61850-9-2LE standard. Note that since the time interval of the numerical scheme is typically smaller than the sampling interval, cubic spline interpolation is utilized to complete the measurement set. Various fault events have been simulated. The available data window is 5 ms after the occurrence of the fault. The absolute fault location error in percentage is defined as the absolute error of fault location divided by the length of the transmission line. Although the actual transmission line parameters in PSCAD/EMTDC are frequency dependent, the parameter matrices utilized by the fault location algorithm are assumed to be frequency independent. Here the parameters at the nominal frequency of 50 Hz are selected as the input parameters for fault location. From the parameters of the transmission line, the value of *Const* is slightly larger than $2\times10^8\ m/s$. To simplify the selection of Δx and Δt, *Const* is set to be $2\times10^8\ m/s$.

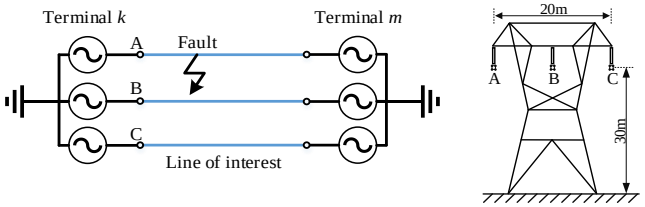

(a) Test system **(b) Tower structure**

Figure. 3. The example test system

A. Validation of Different Schemes by Voltage Distribution

The accuracy of the voltage distributions calculated by three numerical schemes is firstly studied. An internal 0.1 Ω phase A to ground fault occurs close to terminal *m*. The voltage distributions through the entire line are calculated using the three numerical schemes, with three phase voltage and current instantaneous measurements at terminal *k* only. For all three numerical schemes, the distance interval and the time interval are selected as 2 km and 10 μs, satisfying the stable condition of both (13) and (21) but not (8). Note the stable condition of (8) cannot be satisfied with typical selection of intervals.

Figure 4 shows the actual and calculated voltage distributions of phase A at 0.5 ms after fault occurs. From

This article has been accepted for publication in a future issue of this journal, but has not been fully edited. Content may change prior to final publication. Citation information: DOI 10.1109/TPWRD.2020.2974294, IEEE Transactions on Power Delivery

figure, the voltage distribution calculated with the ordinary one-step explicit scheme quickly diverges as the distance increases, while the voltage distributions calculated with Lax-Wendroff and leap-frog schemes are both stable. The results of the leap-frog scheme are closer to the actual voltage distribution.

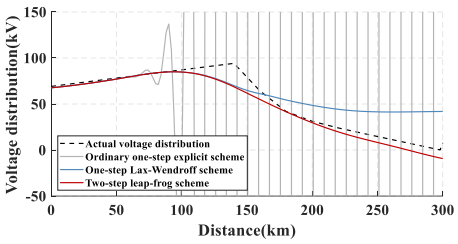

Figure. 4. Voltage distributions calculated with different schemes

B. Validation of Different Schemes by Fault Location

Consider a 0.1 Ω phase A-G fault occurring at 100 km from terminal *k* and at time t = 0.2 s. The voltage and current measurements at both terminals are shown in Figure 5. Apply the proposed leap-frog scheme to the two-iteration fault location algorithm. In iteration 1, the distance interval and the time interval are selected as 2 km and 10 μs. Calculate the voltage distributions during the fault with measurements at each terminal respectively. The value of $f(x,t)$, or the absolute difference between two calculated voltage distributions, is shown in Figure 6 (a). From the figure, the fault location *x* that minimizes $f(x,t)$ at different time steps is around 100 km except the first few time steps. The approximate fault location $l_{f,iteration1}$ from (25) is 100 km and the small transmission line segment for iteration 2 is obtained as [98, 102] km. In iteration 2, the distance interval and the time interval are selected as 100 m and 0.5 μs, which also satisfy (21). The value of $f(x,t)$ is shown in Figure 6 (b). From the figure, the fault location *x* that minimizes $f(x,t)$ at each time step is varying due to the transient of the system. From (25), the fault location is estimated to be 100.1 km.

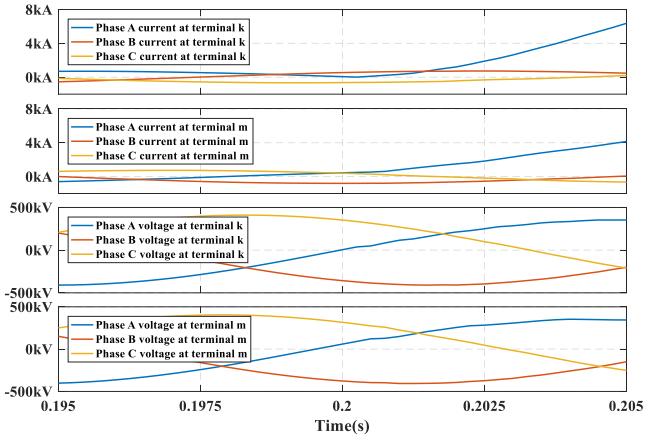

Figure 5. Three phase voltage and current instantaneous measurements during an example 0.1 Ω phase A-G fault (100 km and 0.2 s)

Besides the leap-frog scheme, the fault location results using the Lax-Wendroff schemes are also provided for comparison. The selection of time and distance intervals is: 2 km and 10 μs for iteration 1, and 10 m and 0.5 μs for iteration 2. Here for iteration 2, the distance interval is selected to be even smaller than that of the leap-frog scheme. A group of 0.1 Ω phase A to ground faults occurs at different locations through the entire line. The fault location results are shown in Figure 7 (a). From the figure, although the distance interval of the leap-frog scheme is larger than that of the Lax-Wendroff scheme in iteration 2, the absolute fault location error with the leap-frog scheme is generally smaller. This is exactly because the leap-frog scheme can achieve minimum error with proper selection of distance and time intervals according to (21).

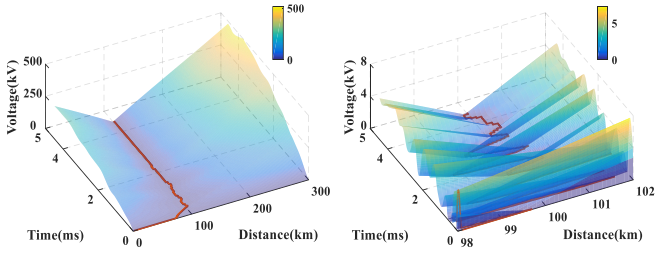

(a) Iteration 1 **(b) Iteration 2**

Figure. 6. Absolute difference between two calculated voltage distributions for 0.1 Ω A-G fault occurs at 100 km

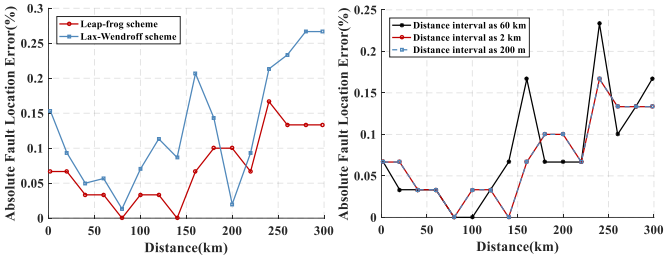

(a) Different numerical schemes **(b) Different distance intervals**

Figure. 7. Absolute fault location errors, 0.1 Ω A-G faults through the entire line

C. Step Number and Calculation Time of the Leap-Frog Scheme

From the error analysis of the leap-frog scheme, once the interval ratio is fixed according to (21), the error of the solution is in direct proportion to the size of the interval. To evaluate the effects of the interval size in the leap-frog scheme, different distance intervals, including 60 km, 2 km and 0.2 km in the first iteration are selected. The distance interval in the second iteration keeps the same (100 m) and the corresponding time intervals in both iterations are selected according to (21). The fault location results of a group of 0.1 Ω phase A to ground faults through the entire line are shown in Figure 7 (b). From the figure, a larger distance interval will usually result in larger absolute fault location error. However, once the interval is small enough (eg. 2 km), the absolute fault location error will not be smaller with smaller interval (eg. 200 m). This is because the absolute fault location errors generated by the numerical solution is too small compare to those due to the inaccuracy of the transmission line PDE model (the PDE model does not consider the frequency dependent parameters of the line). Therefore, such selection of distance interval as 2 km in the first iteration ensures both fault location accuracy and reasonable calculation burden. For the rest of the paper, the distance and time interval are selected as 2 km and 10 μs for the first iteration, and as 100 m and 0.5 μs for the second iteration. Here, the algorithm is implemented in Matlab R2016a on a computer with Intel® i7-7700 CPU. For each fault event, the two-iteration algorithm always finds the fault location within 8 seconds. Since the fault location algorithm is not required to operate in real time, the calculation speed of the proposed fault location algorithm is acceptable in practice.

This article has been accepted for publication in a future issue of this journal, but has not been fully edited. Content may change prior to final publication. Citation information: DOI 10.1109/TPWRD.2020.2974294, IEEE Transactions on Power Delivery

VI. Numerical Validation of the Proposed Method: Comparison to the Existing Fault Location Method

In this section, the fault location results with the proposed method are further validated. The example test system and available measurements are the same as those in section V. Several groups of faults occurring at 0.2 seconds, with different fault types, fault locations and fault impedances are considered. Due to space limitations, here the results of only 5 test cases (240 fault events in total) are shown. For test case 1 to 4, the low impedance phase A to ground faults, phase A to B faults, phase AB to ground faults and three phase faults with 0.1, 1 and 10 Ω fault impedances are considered respectively. For test case 5, high impedance phase A to ground faults with 50, 200 and 500 Ω fault impedances are considered respectively. The fault locations are through the entire length of the transmission line (16 fault locations, 2 km, 298 km, and every 20 km from [20, 280] km from terminal *k*).

The proposed method is compared to the existing time domain voltage method, which utilizes the Bergeron model and the Clarke transformation to calculate the voltage distribution and finds the fault location [5]. Note that here the conventional phasor domain impedance based fault location methods are not considered for comparison, since the accuracy of the calculated phasors could be greatly compromised with the data window of only 5 ms. In addition, the conventional traveling wave methods are not considered for comparison, since the sampling rate of 4 kilo-samples per second is too low for estimating the fault location with reasonable accuracy.

Test Case 1: Low Impedance Phase A to Ground Faults

The fault location results of low impedance phase A to ground faults are shown in Figure 8 (a). The average absolute errors and maximum absolute errors of the proposed method with 0.1, 1 and 10 Ω fault impedances are 0.07%, 0.07%, 0.07%, and 0.17%, 0.17%, 0.17%, respectively. The average absolute errors and maximum absolute errors of the existing method with 0.1, 1 and 10 Ω fault impedances are 0.87%, 0.89%, 1.12%, and 1.30%, 1.30%, 1.60%, respectively.

Test Case 2: Low Impedance Phase A to B Faults

The fault location results of low impedance phase A to B faults are shown in Figure 8 (b). The average absolute errors and maximum absolute errors of the proposed method with 0.1, 1 and 10 Ω fault impedances are 0.31%, 0.25%, 0.26% and 1.03%, 1.33%, 1.20%, respectively. The average absolute errors and maximum absolute errors of the existing method with 0.1, 1 and 10 Ω fault impedances are 0.60%, 0.75%, 0.83%, and 1.57%, 1.43%, 1.50%, respectively.

Test Case 3: Low Impedance Phase AB to Ground Faults

The fault location results of low impedance phase AB to ground faults are shown in Figure 8 (c). The average absolute errors and maximum absolute errors of the proposed method with 0.1, 1 and 10 Ω fault impedances are 0.28%, 0.27%, 0.27% and 1.37%, 1.37%, 1.13%, respectively. The average absolute errors and maximum absolute errors of the existing method with 0.1, 1 and 10 Ω fault impedances are 0.77%, 0.79%, 0.88%, and 1.50%, 1.57%, 1.57%, respectively.

Test Case 4: Low Impedance Three Phase Faults

The fault location results of low impedance three phase faults are shown in Figure 8 (d). The average absolute errors and maximum absolute errors of the proposed method with 0.1, 1 and 10 Ω fault impedances are 0.20%, 0.19%, 0.16%, and 0.83%, 0.80%, 0.73%, respectively. The average absolute errors and maximum absolute errors of the existing method with 0.1, 1 and 10 Ω fault impedances are 0.79%, 0.78%, 0.83%, and 1.97%, 1.93%, 1.77%, respectively.

Test Case 5: High Impedance Phase A to Ground Faults

The fault location results of high impedance phase A to ground faults are shown in Figure 8 (e). The average absolute errors and maximum absolute errors of the proposed method with 50, 200 and 500 Ω fault impedances are 0.06%, 0.05%, 0.07%, and 0.20%, 0.17%, 0.20%, respectively. The average absolute errors and maximum absolute errors of the existing

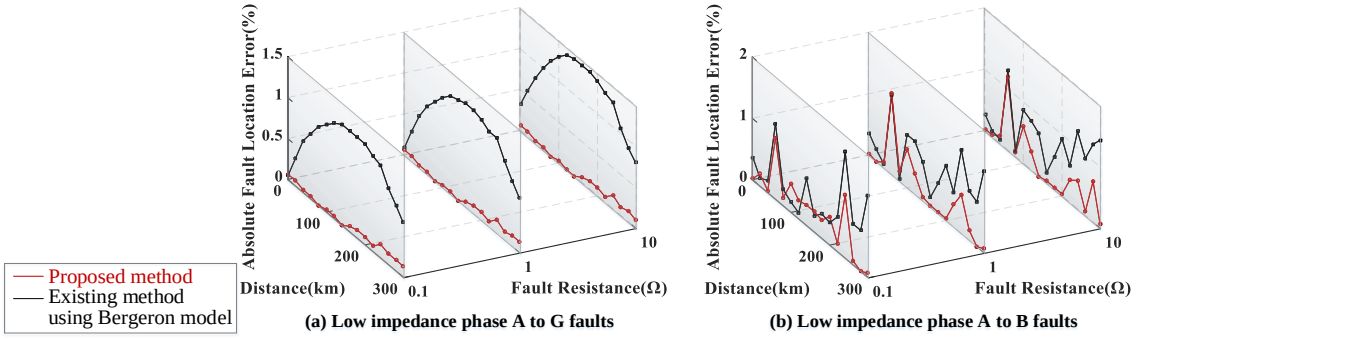

(a) Low impedance phase A to G faults

(b) Low impedance phase A to B faults

(c) Low impedance phase A, B to G faults

(d) Low impedance three phase faults

(e) High impedance phase A to ground faults

Figure. 8. Absolute fault location errors with different fault types, fault locations and fault impedances

This article has been accepted for publication in a future issue of this journal, but has not been fully edited. Content may change prior to final publication. Citation information: DOI 10.1109/TPWRD.2020.2974294, IEEE Transactions on Power Delivery

method with 50, 200 and 500 Ω fault impedances are 2.08%, 5.29%, 10.18%, and 2.63%, 6.63%, 13.97%, respectively.

To sum up, it can be concluded that the proposed method presents higher fault location accuracy compared to the existing Bergeron model based voltage method in above test cases.

VII. Discussion

In this section, the effects of different factors on the fault location accuracy are further discussed, including the fault inception angle, the loading condition, the measurement error, the parameter error and the sampling rate. The example test system and available measurements are the same as those in section V. Other discussions as well as the future work are also presented.

A. *Effect of Fault Inception Angle*

A group of 0.1 Ω phase A to ground faults with 0°, 45° and 90° fault inception angles is studied. The absolute fault location errors are shown in Figure 9 (a). The average absolute errors and maximum absolute errors of the proposed method with 0°, 45° and 90° fault inception angles are 0.07%, 0.15%, 0.28% and 0.17%, 0.47%, 0.67%, respectively. The average absolute errors and maximum absolute errors of the existing method with 0°, 45° and 90° fault inception angles are 0.87%, 0.74%, 0.64% and 1.30%, 1.30%, 1.40%, respectively. Here the 0° fault inception angle corresponds to zero phase A voltage when the fault occurs, while a 90° fault inception angle corresponds to maximum phase A voltage when the fault occurs. Compare to the waveform in Figure 8 (a), one can observe that the fault location error increases with larger inception angles. This is because the voltage/current waveforms contain rich frequency information especially during severe transients (caused by large inception angles), and the proposed fault location method does not consider frequency dependent parameters.

B. *Effect of Loading Condition*

A group of 0.1 Ω phase A to ground faults with different loading conditions is studied. The different loading condition is simulated with different phase angle differences between two equivalent sources at terminals of the line, including 10°, 20°, 30°, 40° and 50°, respectively. The absolute fault location errors are shown in Figure 9 (b). The average absolute errors and maximum absolute errors of the proposed method with 10°, 20°, 30°, 40° and 50° phase difference are 0.07%, 0.07%, 0.07%, 0.07%, 0.08% and 0.13%, 0.17%, 0.17%, 0.20%, 0.20%, respectively. The average absolute errors and maximum absolute errors of the existing method with 10°, 20°, 30°, 40° and 50° phase difference are 0.49%, 0.92%, 1.36%, 1.82%, 2.28% and 0.67%, 1.23%, 1.83%, 2.53%, 3.20%, respectively.

C. *Effect of Measurement Error*

A group of 0.1 Ω phase A to ground faults with different measurement errors is studied. The measurement error is added in the fault location algorithm by changing the original measurements. The measurement errors are assumed to obey the Gaussian distribution with the standard deviation of 0.5%, 1% and 2%, respectively. The absolute fault location errors are shown in Figure 9 (c). The average absolute errors and maximum absolute errors of the proposed method with 0.5%, 1% and 2% measurement errors are 0.11%, 0.15%, 0.25% and 0.23%, 0.30%, 0.50%, respectively. The average absolute errors and maximum absolute errors of the existing method with 0.5%, 1% and 2% measurement errors are 1.00%, 1.08%, 1.20% and 1.47%, 1.73%, 1.97%, respectively.

D. *Effect of Parameter Error*

A group of 0.1 Ω phase A to ground faults with different parameter errors is studied. The 0.5%, 1% and 2% parameter errors are added to all parameter matrices of the transmission line respectively in the fault location algorithm (the example

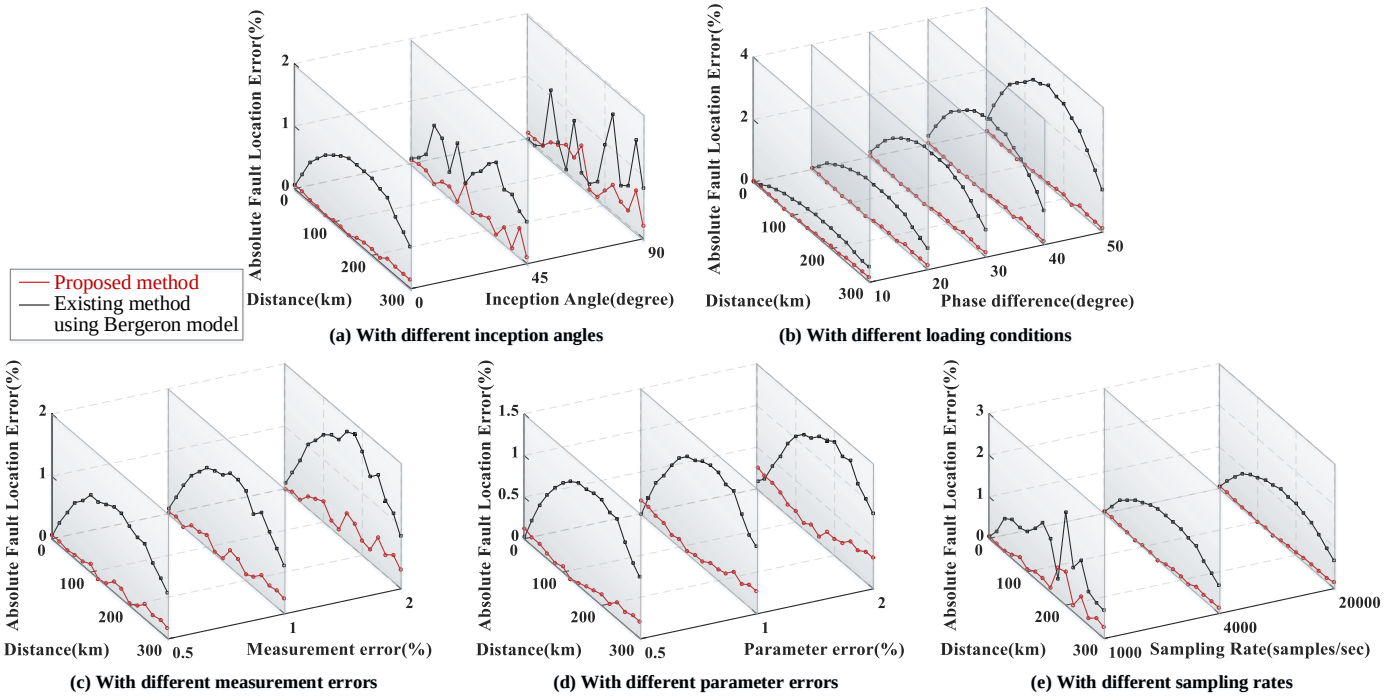

Figure. 9. Absolute fault location errors of phase A to G faults with different factors

test system in PSCAD/EMTDC remains unchanged). The absolute fault location errors are shown in Figure 9 (d). The average absolute errors and maximum absolute errors of the proposed method with 0.5%, 1% and 2% parameter errors are 0.11%, 0.15%, 0.22% and 0.20%, 0.27%, 0.37%, respectively. The average absolute errors and maximum absolute errors of the existing method with 0.5%, 1% and 2% parameter errors are 0.92%, 0.91%, 0.94% and 1.30%, 1.30%, 1.56%, respectively.

E. Effect of Sampling Rate

A group of 0.1 Ω phase A to ground faults with the sampling rates of 1k, 4k and 20k samples per second is studied. The absolute fault location errors are shown in Figure 9 (e). The average absolute errors and maximum absolute errors of the proposed method with 1k, 4k and 20k sampling rates are 0.25%, 0.07%, 0.06% and 0.80%, 0.17%, 0.13%, respectively. The average absolute errors and maximum absolute errors of the existing method with 1k, 4k and 20k sampling rates are 0.98%, 0.87%, 0.86% and 2.43%, 1.30%, 1.30%, respectively. One can observe that higher sampling rates will not largely improve the fault location accuracy of the proposed method. The sampling rate of 4k samples per second is recommended as it is consistent with the IEC 61850-9-2LE standard and in this case the error of the proposed method is sufficiently small.

F. Other Discussions and Future Work

The numerical experiments in this paper only demonstrate the results in three phase overhead transmission lines. Actually, the proposed fault location methodology could be similarly applied to multi-phase/multi-circuit AC/DC overhead transmission lines or underground cables. The detailed verification of the proposed methodology in complex systems with asymmetrical and nonhomogeneous AC/DC overhead lines and underground cables is still required and will be covered in future publications. In addition, the proposed fault location method holds the following two important assumptions. First, the transmission line parameter matrices are frequency independent constants and accurately known. Second, the terminal voltage and current instantaneous measurements are available and accurate. For the first assumption, the fault location errors could be generated especially during severe transients or with large transmission line parameter errors. In this case, frequency dependent parameter models of transmission lines as well as online parameter identification approaches could be considered to improve the performance of the proposed method. For the second assumption, measurement errors, especially systematic measurement errors due to PTs and CTs, may also generate fault location error. Therefore, detailed modeling of PTs and CTs may be required to accurately recover the primary side voltage and current signals. Finally, validation through real world data will be valuable to ensure the practicability of the proposed method. These issues will also be carefully studied in future publications.

VIII. Conclusion

This paper proposes a time-domain fault location method that can be applied for transmission lines with high-speed tripping techniques. The sampling rate of the method is recommended as 80 samples per cycle to be compatible with IEC 61850-9-2LE standard in present digital substations. A numerical scheme is first proposed to accurately solve the voltage distribution through the transmission line. The optimal selection of time and distance interval is mathematically proved to ensure stability and minimum solution error of the numerical scheme. The fault location can be afterwards obtained by finding the extremum value of the voltage distribution. The distributed parameters and the asymmetry of the transmission line are fully considered. Numerical experiments validate the effectiveness of the proposed numerical scheme with comparison to other considered numerical schemes. In addition, the proposed fault location method has higher fault location accuracy compared to the existing Bergeron model based voltage method, with different fault types, locations and impedances. The method also demonstrates its effectiveness with different fault inception angles, loading conditions, measurement errors and parameter errors.

References

[1] S. Das, S. Santoso, A. Gaikwad and M. Patel., "Impedance-based fault location in transmission networks: theory and application," *IEEE Access*, vol. 2, pp. 537– 557, Feb. 2014.

[2] S. M. Brahma and A. A. Girgis, "Fault location on a transmission line using synchronized voltage measurements," *IEEE Trans. Power Del.*, vol. 19, no. 4, pp. 1619-1622, Oct. 2004.

[3] N. Kang, J. Chen and Y. Liao, "A Fault-Location algorithm for series-compensated double-circuit transmission lines using the distributed parameter line model" *IEEE Trans. Power Del.*, vol. 30, no. 1, pp. 360-367, Feb. 2015.

[4] Y. Liu, B. Wang, X. Zheng, D. Lu, M. Fu and N. Tai, "Fault location algorithm for non-homogeneous transmission lines considering line asymmetry", *IEEE Trans. Power Del.*, 2020, early access.

[5] G. Song, J. Suonan, Q. Xu, P. Chen, and Y. Ge, "Parallel transmission lines fault location algorithm based on differential component net," *IEEE Trans. Power Del.*, vol. 20, no. 4, pp. 2396-2406, Oct. 2005.

[6] IEEE guide for determining fault location on AC transmission and distribution lines, IEEE Standard C37.114, 2014.

[7] F. H. Magnago and A. Abur, "Fault location using wavelets, " *IEEE Trans. Power Del.*, vol. 13, no. 4, pp. 1475–1480, Oct. 1998.

[8] C. Zhang, G. Song, T. Wang and L. Yang, "Single-Ended traveling wave fault location method in DC transmission line based on wave front information," *IEEE Trans. Power Del.*, vol. 34, no. 5, pp. 2028-2038, Oct. 2019.

[9] C.Y. Evrenosoglu amd A. Abur, "Travelling wave based fault location for teed circuits," *IEEE Trans. Power Del.*, vol. 20, no. 2, pp. 1115–1121, Apr. 2005.

[10] O. M. K. K. Nanayakkara, A. D. Rajapakse and R. Wachal, "Traveling-wave-based line fault location in star-connected multiterminal HVDC systems," *IEEE Trans. Power Del.*, vol. 27, no. 4, pp. 2286–2294, Jul. 2012.

[11] F. V. Lopes, K. M. Dantas, K. M. Silva and F. B. Costa, "Accurate two-terminal transmission line fault location using traveling waves," *IEEE Trans. Power Del.*, vol. 33, no. 2, pp. 873-880, Apr. 2018.

[12] Y. Liu, S. Meliopoulos, N. Tai, L. Sun and B. Xie, "Protection and fault locating method of series compensated lines by wavelet based energy traveling wave," *IEEE Power Energy Soc. Gen. Meet.*, Chicago, IL, USA, 2017.

[13] V. V. Terzija and Z. M. Radojevic´, "Numerical algorithm for adaptive autoreclosure and protection of medium-voltage overhead lines," *IEEE Trans. Power Del.*, vol. 19, no. 2, pp. 554-559, Apr. 2004.

[14] Y. Liu, S. Meliopoulos, Z. Tan, L. Sun and R. Fan, "Dynamic state estimation-based fault locating on transmission lines," *IET Generation Transmission Distribution*, vol. 11, no. 17, pp. 4184-4192, Nov. 2017.

[15] R. Fan, Y. Liu, R. Huang, R. Diao and S. Wang, "Precise Fault Location on Transmission Lines Using Ensemble Kalman Filter", *IEEE Trans Power Del.*, vol. 33, no. 6, pp. 3252-3255, Dec. 2018.

[16] A. Gopalakrishnan, M. Kezunovic, S. M. McKenna, and D. M. Hamai, "Fault location using the distributed parameter transmission line model," *IEEE Trans. Power Del.*, vol. 15, no. 4, pp. 1169-1174, Oct. 2000.

[17] J. Suonan, S. Gao, G. Song, Z. Jiao and X. Kang, " A novel fault-location method for HVDC transmission lines" *IEEE Trans. Power Del.*, vol. 25, no. 2, pp. 1203-1209, Apr. 2010.

[18] M. Davoudi, J. Sadeh and E. Kamyab, "Transient-based fault location on three-terminal and tapped transmission lines not requiring line parameters," *IEEE Trans. Power Del.*, vol. 33, no. 1, pp. 179-188, Feb. 2018.
[19] A. R. Djordjevic and R. F. Harrington, "Time-domain response of multiconductor transmission lines," *Proc. IEEE*, vol. 75, no. 6, pp. 743-764, Jun. 1987.
[20] C. R. Paul, "Incorporation of terminal constraints in the FDTD analysis of Transmission Lines," *IEEE Trans. Electromagn. Compat.*, vol. 36, no. 2, pp. 85-91, May. 1994.
[21] K. W. Morton and D. F. Mayers, "Numerical solution of partial differential equations," New York, NY, USA: Cambridge Univ. Press 2005.
[22] H. W. Dommel, "Digital computer solution of electromagnetic transients in single-and multiphase networks," *IEEE Trans. Power App. Syst.*, vol PAS-88, no. 4, pp. 388-399, Apr. 1969.

BIOGRAPHIES

Dayou Lu (S'19) received the B.S. in Electrical Engineering and Automation from Huazhong University of Science and Technology, Wuhan, Hubei, China, in 2017. He is currently working towards the Ph.D. degree in Electrical Engineering, in the School of Information Science and Technology, ShanghaiTech University, Shanghai, China. His research interests include modeling, protection and fault location of transmission lines.

Yu Liu (S'15-M'17) received the B.S. and M.S. in electrical power engineering from Shanghai Jiao Tong University, Shanghai, China, in 2011 and 2013, respectively, and the Ph.D. degree in electrical and computer engineering from Georgia Institute of Technology, Atlanta, GA, USA, in 2017. He is currently a Tenure-Track Assistant Professor with the School of Information Science and Technology, ShanghaiTech University, Shanghai, China. His research interests include modeling, protection, fault location, and state/parameter estimation of power systems and power electronic systems.

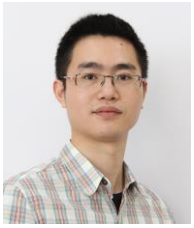

Qifeng Liao received the Ph.D. degree in applied numerical computing from the School of Mathematics, The University of Manchester, in December 2010. From January 2011 to June 2012, he held a postdoctoral position at the Department of Computer Science, University of Maryland, College Park. From July 2012 to February 2015, he held a postdoctoral position at the Department of Aeronautics and Astronautics, Massachusetts Institute of Technology. He is currently an Assistant Professor with the School of Information Science and Technology, ShanghaiTech University. His research interest includes effcient numerical methods for PDEs with high-dimensional random inputs, and his work was supported by the National Natural Science of China and Shanghai Young East Scholar.

Binglin Wang (S'19) received the B.S. in Electrical Engineering and Intelligent Control from Xi'an University of Technology, Xi'an, Shaanxi, China, in 2018. He is currently working towards the Ph.D. degree in Electrical Engineering, in the School of Information Science and Technology, ShanghaiTech University, Shanghai, China. His research interests include protection, fault location and state estimation of HVAC and HVDC transmission lines.

Wentao Huang (S'15-M'16) was born in Anhui, China, in 1988. He received the Ph.D. degree in electrical engineering from Shanghai Jiao Tong University, Shanghai, China, in 2015. He is currently an associate professor with the Department of Power Electrical Engineering, Shanghai Jiao Tong University. He is the associate director of Key Laboratory of Control of Power Transmission and Conversion, Ministry of Education of China. His research interests include protection and control of active distribution systems, microgrids and integrated power systems for marines.

Xinze Xi received the B.S. degree in automation from Wuhan University, Wuhan, China, in 2010, and the Ph.D. degree in control theory and application from Tsinghua University, Beijing, China, in 2016. From 2016 to 2018, he was a Postdoctoral Research Fellow with the Electric Power Research Institute, Yunnan Power Grid Co., Ltd., China Southern Power Grid, Kunming, China. His current research interests include grid integration of renewable energy conversion systems, power system stability analysis and control.